

Article

Development and Real-Time Performance Evaluation of Energy Management Strategy for a Dynamic Positioning Hybrid Electric Marine Vessel

Truong M. N. Bui ^{1,*} , Truong Q. Dinh ¹, James Marco ¹ and Chris Watts ²

¹ Energy Innovation Centre, WMG, University of Warwick, Coventry CV4 7AL, UK; t.dinh@warwick.ac.uk (T.Q.D.); james.marco@warwick.ac.uk (J.M.)

² Babcock International Group, Leicester LE3 1UF, UK; chris.watts@babcockinternational.com

* Correspondence: truong.bui@warwick.ac.uk; Tel.: +44-24-765-75855

Abstract: Hybridisation of energy sources in marine vessels has been recognized as one of the feasible solutions to improve fuel economy and achieve global emission reduction targets in the maritime sector. However, the overall performance of a hybrid vessel system is strongly dependent on the efficiency of the energy management system (EMS) that regulates the power-flow amongst the propulsion sources and the energy storage system (ESS). This study develops a simple but production-feasible and efficient EMS for a dynamic positioning (DP) hybrid electric marine vessel (HEMV) and real-time experimental evaluation within a hardware-in-the-loop (HIL) simulation environment. To support the development and evaluation, map-based performance models of HEMVs' key components are developed. Control logics that underpin the EMS are then designed and verified. Real-time performance evaluation to assess the performance and applicability of the proposed EMS is conducted, showing the improvement over those of the conventional control strategies. The comparison using key performance indicators (KPIs) demonstrates that the proposed EMS could achieve up to 4.8% fuel saving per voyage, while the overall system performance remains unchanged as compared to that of the conventional vessel.

Keywords: hybrid electric propulsion system; energy management strategy; dynamic positioning marine vessel; map-based performance model; real-time verification



Citation: Bui, T.M.N.; Dinh, T.Q.; Marco, J.; Watts, C. Development and Real-Time Performance Evaluation of Energy Management Strategy for a Dynamic Positioning Hybrid Electric Marine Vessel. *Electronics* **2021**, *10*, 1280. <https://doi.org/10.3390/electronics10111280>

Academic Editors: Cheng Siong Chin and Hamid Reza Karimi

Received: 19 April 2021

Accepted: 25 May 2021

Published: 27 May 2021

Publisher's Note: MDPI stays neutral with regard to jurisdictional claims in published maps and institutional affiliations.



Copyright: © 2021 by the authors. Licensee MDPI, Basel, Switzerland. This article is an open access article distributed under the terms and conditions of the Creative Commons Attribution (CC BY) license (<https://creativecommons.org/licenses/by/4.0/>).

1. Introduction

In the maritime transport sector, ships are identified as the most efficient transport means for heavy freight and cargo transportation. Conventional marine vessels, which utilise a traditional internal combustion engine (ICE) as a main propulsion system, are very noticeable with high fuel consumption, low fuel economy, and large exhaust emissions, comprising carbon dioxide (CO₂) and particulate matter, that produce harmful impacts to the environment [1–4]. Since recent regulations [5] agreed upon by the International Maritime Organization (IMO) and the European Union (EU) have required significant reduction of exhaust emissions to prevent air pollution of ships, many ship-building manufacturers have been forced to reduce the operating speed as an immediate measure of reducing fuel consumption, hence lowering gas emissions [6]. Other approaches have focused on developing new propulsion technologies and suggested feasible energy management solutions to cut down environmental pollution, reduce CO₂ emissions, and maximise fuel efficiency for many kinds of shipping transportation [7].

One practical and feasible solution to address these concerns is the hybridisation of the vessel's propulsion systems. The hybridisation is based on the combination of diesel-generator-powered (DG) electric propulsion systems and optimal energy storage systems (ESSs), accompanied by advanced control strategies of energy management systems (EMSs) to regulate the power-flow between DG and ESSs. Although the electrical-powered

propulsion systems have been introduced throughout the world in the early 1990s, offering benefits over mechanical propulsion systems in terms of fuel economy, emissions, and maintenance loads, hybrid electric propulsion systems (HEPSs) have just been introduced to numerous applications of automotive industry sector recently [8–10]. However, in the maritime industry sector, the development of HEPSs for vessels is just at the commencement of its exploration [4,11–13]. They are attracting research intention in both academia and industry, especially with regard to the integration of battery storage systems (BSSs) into the system as well as the development of achievable EMS to lower fuel consumption and gas emissions. Recently, extensive studies have been reported on high power efficiency ships using new hybrid propulsion technologies and competency EMS [14–16]. Jaurola et al. [14] suggested an optimising design tool for the power management system of a marine vessel based on a literature review. The article presented a key idea focusing on the EMS development, which allows individual power sources to run closer to their optimal output power. However, the study is a purely theoretical investigation, and there is no simulation or experimental result carried out. Kanellopoulos et al. [17] investigated the application of a HEPS in an offshore construction support vessel. An electromotive force control approach was designed based on the IF-ELSE logics and look-up tables to determine suitable actions for the system. From the load flow analysis, it is shown that the hybrid system is more flexible in providing the necessary loads under certain operational conditions. The simulation results illustrated the improvement in reducing pollutant exhaust gas emissions and noise levels on board. Practical comparison of the system is necessary to evaluate the system performance in real-time. Diju et al. [18] studied HEPS for inland waterway vessels and developed a three-layer logic threshold control method for the system to reduce the fuel consumption and gas emission. The simulation results show the improvement of the fuel economy as compared to that of the fuzzy logic strategy. In general, the main control objective of the control strategies for hybrid ships is to allow the engines to operate near to their highest working efficiency point or lowest emission point for a given operating speed within a particular load profile. This limits the operational capacity of the system within a specific profile while there is considerable diversity in the operational capability. Furthermore, the control performance of the discussed hybrid systems was evaluated via simulation methods based on limited load profiles and operating conditions, and real-time validation is necessary to evaluate the performance of those approaches. In fact, the implementation of HEPS is mostly restricted to certain types of vessels, as it is particularly applicable in cases where the mean propulsion power demand is significantly lower than the installed capacity [17]. The performance of a HEPS is also limited to its operating load profile where the influence of load changes can be addressed by the optimal EMS. However, due to the diversity of working conditions and the complexity of control systems, efficient EMS design and verification concerns for the HEPS still draw significant attention from researchers.

Notwithstanding, real-time verification of a complete HEPS with EMS remains challenging due to the high capital cost of prototype development, time consumption, and safety concerns, etc. The hardware-in-the-loop (HIL) simulation technique, which has been intensively used in many fields such as control development and verification, product and component assessment, and system performance validation [19–22], seems to be the most favourable method for real-time testing and evaluating the system. It enables the testing of actual components in conjunction with a virtual computer-based simulation model to represent parts of the system. This testing method avoids complex processes in hardware setup and time constraints and helps lower the risks to people and equipment. The novelties and contributions of this study are summarized as follows. First, the approach establishes an applicable methodology to conduct simulation and verification of the EMS on a prototype of dynamic positioning (DP) hybrid electric marine vessel (HEMV) application in a real-time environment. The method provides the ability to apply HIL techniques in constructing a real-time HEMV system and to transfer the advantages of HIL technology, which are very well documented and researched within the automotive and

aerospace domains, to the marine sector for real-time validation, evaluation, and verification. Thus, it can be the premise for the development, verification, and deployment of the next generation of hybridization and electrification of marine vessels. Second, a simple but production-feasible and efficient EMS, which is able to deal with different operating modes of HEMV application enhancing the fuel economy and reducing environmental emissions, is developed to overcome the drawbacks of traditional control approaches in terms of efficiency and performance. Third, the successful deployment of a real-time battery simulator (BAT-S), which represents the complete BSS, extends the applicability of the traditional HIL testing method for testing and evaluating the performance of the EMS. The BAT-S has been completely integrated into the system to evaluate the control strategies instead of using a physical BSS that has obviously high costs, testing time, and safety concerns. Finally, as a technical transfer method from the automotive to maritime sector, a HIL-based DP HEMV platform is built for the experimental evaluation of EMS in a real-time testing environment. The achievable HIL simulator platform can potentially provide the capability of evaluating the EMS under any drive cycles with different operational modes of DP marine vessels.

The remainder of the paper is organised as follows. The system architecture and representative plant model are introduced in Section 2. The modelling of key components of the DP HEMV system is presented in Section 3. In Section 4, an extended rule-based control (ERBC) scheme is developed as a feasible control logic based on the principle of load levelling to control the power flow amongst the energy sources of the system. In this section, other rule-based control schemes, e.g., conventional DG control (DGC) and standard rule-based control (RBC), are also developed for comparison purposes. Then, a real-time HIL simulation platform is built in Section 5 to enable real-time simulation and evaluation of the control system. In Section 6, experimental comparison of the system with different control strategies is carried out to access the control performance of the employed HEMV system and the operational ability of the EMS in a real-time environment. Finally, the conclusion and future works are presented in Section 7.

2. DP HEMV System Description

Dynamic positioning in the maritime industry is known as a control procedure that automatically maintains the vessel and ship position and heading direction by using its own propellers and thrusters [23]. A ship equipped with this kind of automatic control system offers a capability of holding itself stationary while retaining performance for other tasks. This is therefore relevant for the vessel when mooring or anchoring at sea or in a deep-water area or wherever a DP operation is needed. Since the DP system has recently been increased in the maritime industry, different types of shipping vessels are being fitted with a DP system to enhance the control performance and handling characteristics of the vessels [24]. However, similar to the hybrid propulsion ships, DP vessels require effective EMS due to the complexity and diversity in the control system in order to manage the operational sequence of various power sources in the vessel so that they can perform well while maintaining DP operation.

In fact, the operation of DP vessels generally consists of seven modes: harbour, harbour loading, transit (or cruising), DP loading, DP standby, emergency, and black start [25,26]. To guarantee the vessel performance within its operation modes as well as to maintain the capability to respond quickly to peak loads, the traditional propulsion system needs to have a power capacity much higher than the average power required to operate the vessel. This leads to the fact that the vessel would be equipped with large size engine-generators while normally operating in low power modes or at low efficiency regions, therefore resulting in high fuel consumption and thus gas emissions [26]. Hence, a hybrid propulsion system should be employed, replacing the traditional one, to overcome these restrictions. Subsequently, an efficient EMS for hybrid propulsion systems should be developed as an urgent demand to improve the environmental impacts and performance of DP vessels.

In this study, a series alternating current (AC) DP HEMV is chosen as the target system for the verification and evaluation of the developed EMS. The architecture diagram of the employed HEMV is illustrated in Figure 1. The system principally consists of two DG units, a battery pack representing the ESS, two AC propulsion motors, power converters, transformers, and auxiliary and hotel loads. In each DG, a diesel ICE is engaged to drive the AC generator that acts as the main power source to produce electric power for the common AC grid. In this system, the AC generator is a synchronous machine, which means the output frequency of the generator is dependent upon its rotation speed; the operating frequency of each DG is therefore required to be constant to maintain the grid operating frequency. Consequently, the diesel ICE must be maintained at a constant speed as well. The operation parameters of the DG used in this study are listed in Table 1 [25]. The lithium-ion battery-based ESS is utilised to store the excess electric energy from the grid when available and release that to the grid when requested. By using the transformers and converters, the energy in the common AC bus provided by the DGs and ESS is then converted and distributed to consumers such as propulsion motors and all other system loads.

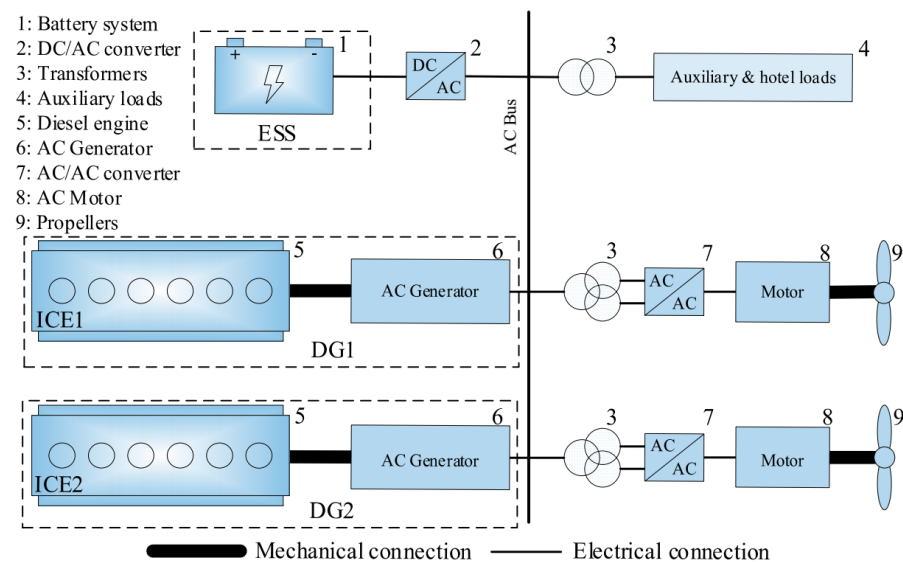


Figure 1. Structure of the employed HEMV system.

Table 1. DG's parameters.

Parameter	Value	Unit
Number of DG	2	-
Maximum output power (@2200 rpm)	533	kW
AC generator's working frequency	60	Hz
Number of poles of the generator	4	-
Working speed	1800	rpm

3. DP HEMV System Modelling

In this section, the DP HEMV is built as the combination of key components' sub-models, comprising the DG, battery ESS system, and power electronics, while other supplement components are ignored or assumed unaffected. To cut down the complexity of the system model as well as to support the EMS development and verification, the following key assumptions are applied:

- (1) The speed, torque, and output power of the ICE are properly defined as in Table 1 to fit the laboratory testing condition. The pre-defined ICE parameters are based on the proper selection and combination of commercial Tier 4 marine engines from JCB Ltd. and Caterpillar Ltd. marine engine manufacturers, which are detailed in [27,28].
- (2) The efficiency and variation sensitivity of the propellers are unchanged. Hence, the efficiency is expected to be ideal and set to 100% (there is no deficit of power or performance).
- (3) Depending on the actual torque and total power request, the fuel consumption of each diesel ICE is calculated based on a fuel consumption map; likewise, the performance of each AC generator is interpolated based on an efficiency map.
- (4) Total measurement accuracy and power loss through power electronic equipment within the AC grid is assumed constant and expressed by an efficiency coefficient.
- (5) The transient behaviours of the battery-based ESS during dynamic cycling are neglected. Thus, a simple battery empirical model is feasible for the control verification.
- (6) Negative influence of temperature on the performance of the ESS and overall HEMV system are not considered in this study.
- (7) The influences of battery degradation on the control performances are ignored; hence, the battery performance remains unchanged during the operation.
- (8) The propulsion and auxiliary and hotel loads are represented by total operation power request, which is already merged into the load profile.

3.1. Diesel Engine-Generator Modelling

The steady-state output power of the selected ICE is easily calculated via a two-dimensional function look-up table to map the inputs of engine speed and torque to its output power. Figure 2 illustrates the relationship of the ICE output power and torque versus its operational speed, which demonstrates the performance of the selected diesel ICE. Depending on the actual operational speed and the torque request, the output power of the ICE can be obtained. The output power of the generator can be therefore calculated based on an efficiency factor of the generator.

$$P_{gen} = P_{eng}\eta_{gen} \quad (1)$$

where P_{eng} is the output power of the ICE (kW); P_{gen} is the output power of the generator (kW); η_{gen} is the efficiency factor, which is calculated based on the efficiency map of the AC generator.

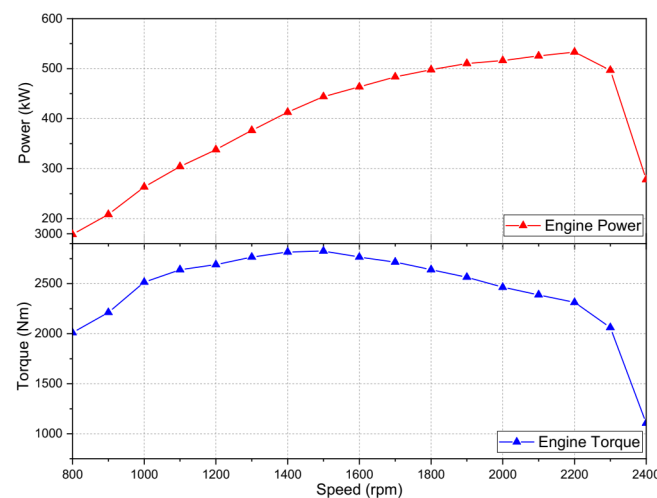


Figure 2. ICE output power and torque versus speed.

Likewise, the ICE fuel consumption is derived from a brake-specific fuel consumption (BSFC) map versus engine torque and speed, as shown in Figure 3. This figure depicts an optimal operating line (OOL) and maximum operating line (MOL) of the ICE that represent the output power limit of the ICE when running at the optimum and maximum operational curves, respectively. They are calculated based on the power maps of the reference engines in the assumptions. Here, the OOL (blue dash-line) indicates the best energy efficiency of the ICE, while the MOL (red dash-line) offers the maximum output power of the engine. In any type of engine, OOL is a set of optimal operational points (OOP), based on engine speed and torque, at which the highest energy efficiency can be delivered. Similarly, MOL is a set of maximum operating points (MOP) where the engine provides maximum output power according to actual engine speed and torque. The instantaneous fuel consumption rate can be calculated as follows:

$$M_{eng} = BSFC \frac{P_{eng} 10^{-3}}{\rho} \tag{2}$$

where M_{eng} is the instantaneous fuel consumption rate (L/h); $BSFC$ is the brake-specific fuel consumption (g/kWh); P_{eng} is the output power of the ICE (kW); ρ is the diesel fuel density ($\rho = 0.84$ kg/L).

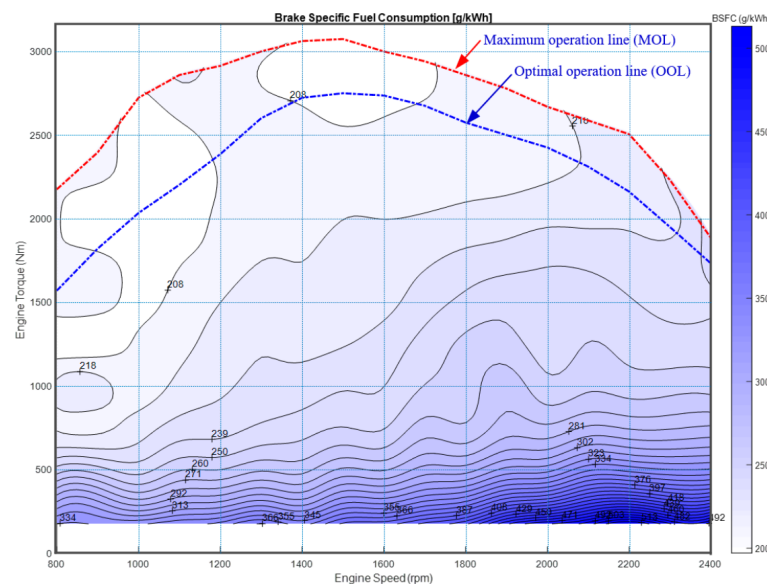


Figure 3. BSFC map of the selected diesel ICE.

Consequently, the fuel consumption is determined by the integration of the instantaneous fuel consumption rate over time as follows:

$$f_{fuel}(t) = \int_0^t M_{eng}(t)dt \tag{3}$$

3.2. Battery Modelling

The battery pack plays an important role in a HEMV. It acts as the ESS of the vessel system, providing the capability of storing excess electrical energy when the total power generated by the DGs exceeds the load demand. The battery is also able to release electrical energy to the grid when the load demand is greater than the total power provided by the internal DGs. In this circumstance, the battery pack acts as a second power source that supplies extra energy to fulfil the system power. In the literature, different types of battery chemicals are used as a dominant energy source, such as lithium-ion, nickel–cadmium, lead-acid, and alkaline. Amongst them, lithium-ion batteries are the most competitive

candidate because of their unique features such as their high energy density, long life cycle, high efficiency, and environmental-friendly performance [29]. Recent studies also show that advanced lithium-ion battery models such as the equivalent circuit model (ECM) [30,31] and electrochemical-based battery models [32,33] have been employed in the control design and energy management systems. However, a drawback that remains in such studies is the calculation effort, which has a negative impact on the control performance, especially for real-time feedback control and verification. Hence, depending on the complexity of the battery model and the size of the whole system model, a suitable battery model can be selected to satisfy the calculation constraint of real-time applications.

In this study, a lithium-ion battery type is therefore equipped to regulate any excess or deficit electric power of the employed HEMV. The battery pack is formed by a series of eight identical battery modules, while each module is created by connecting, in series and parallel, Sony lithium-ion cells—US18650VTC6 as of 16S167P configuration, which are 16 cells in series and 167 cells in parallel connected. The employed Sony cell can provide 3.63 V of nominal voltage and 3 Ah of maximum capacity. The key parameters of the employed battery pack are shown in Table 2.

Table 2. Battery parameters.

<i>Battery Parameters</i>	<i>Symbol</i>	<i>Value</i>	<i>Unit</i>
Cell nominal voltage	V_c	3.63	V
Cell capacity	C_c	3	Ah
Battery module (16S167P) nominal voltage	V_m	60	V
Battery module (16S167P) capacity	C_m	500	Ah
Number of battery module in series	-	8	-
Battery pack nominal voltage	V_p	480	V
Battery pack capacity	C_{max}	500	Ah
Peak charging current	I_{ch}^{max}	500	A
Charge efficiency	η_{ch}	90	%
Peak discharging current	I_{dis}^{max}	1000	A
Discharge efficiency	η_{dis}	100	%

The battery model used in this study is inherited from our previous studies [25,26]. The following discussion summarises the essential battery information of an ECM as depicted in Figure 4. The open circuit voltage (OCV) and internal resistance of the battery are the function of battery state of charge (SOC) and temperature that are easy to measure and estimate using experimental characterisation. The battery OCV can be calculated by using the following equation:

$$V_{OC} = I_{bat}R_{bat} + V_t \quad (4)$$

where V_{OC} is the OCV of the battery (V); I_{bat} is the battery current (A); R_{bat} is the battery internal resistance (Ω). V_t is the terminal voltage (V).

The output power of the battery can be calculated as follows:

$$P_{bat} = V_{OC}I_{bat} - I_{bat}^2R_{bat} \quad (5)$$

where P_{bat} is the output power of the battery (W); $I_{bat}^2R_{bat}$ is the power lost factor of the battery and can be approximated by a Coulomb efficiency term: η_{bat} .

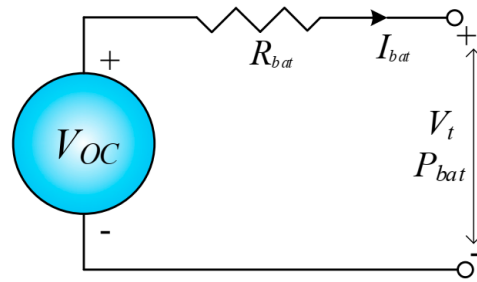


Figure 4. Battery equivalent circuit model.

The battery current and the variation of SOC in the battery can be defined as follows:

$$I_{bat} = \frac{V_{OC} - \sqrt{V_{OC}^2 - 4R_{bat}P_{bat}}}{2R_{bat}} \quad (6)$$

$$\dot{SOC} = -\frac{I_{bat}}{C_{max}} \quad (7)$$

where \dot{SOC} is the variation of the battery SOC (%); C_{max} is the maximum battery capacity (Ah).

The SOC then can be updated for step t^{th} using the Coulomb counting method as follows:

$$SOC(t) = SOC(0) + \int_0^t \frac{I_{bat}(t)}{C_{max}} dt \quad (8)$$

where t is the time taken, $SOC(t)$ is the SOC at time t , and $SOC(0)$ is the initial SOC of the battery.

The OCV–SOC curve and the internal resistance variation versus SOC depicted in Figure 5 are derived based on the characterisation data of three pristine battery cells. The experimental works were carried out at the Energy Innovation Centre (EIC) laboratory, WMG, the University of Warwick, United Kingdom. Before the characterisation was performed, the cells were rested within a thermal chamber at 25 °C, allowing a stabilisation for 12 h. The characterisation test was then conducted through four tests including the capacity measurement, OCV–SOC relationship, and internal resistance measurement through both a pulse power test and electro-chemical impedance spectroscopy (EIS) measurement [34]. The characterisation data describing electrical behaviours of the cells are used to derive the parameters of the battery model.

In fact, for safety purposes, the variation of the battery SOC is limited within its safety operational range. This is to avoid over-charge or over-discharge during the operation and prolong the lifetime of the battery. Additionally, for testing the system within the laboratory environment and reducing the simulation time effort and capital cost, it is noted that the whole battery pack is simulated by the BAT-S. The battery pack is represented by a battery sub-module, which consists of a single string of 16 cells connected in series as of the 16S1P configuration. This representative battery sub-module can produce 60 V nominal voltage and 3 Ah capacity. It is then scaled-up to represent the complete battery pack of the system, as depicted in Table 2. Table 3 proposes the normal working modes of the battery pack, where SOC stands for the actual state-of-charge level of the battery; SOC_L , SOC_M , and SOC_H represent the low, medium, and high operating thresholds of the battery pack, respectively.

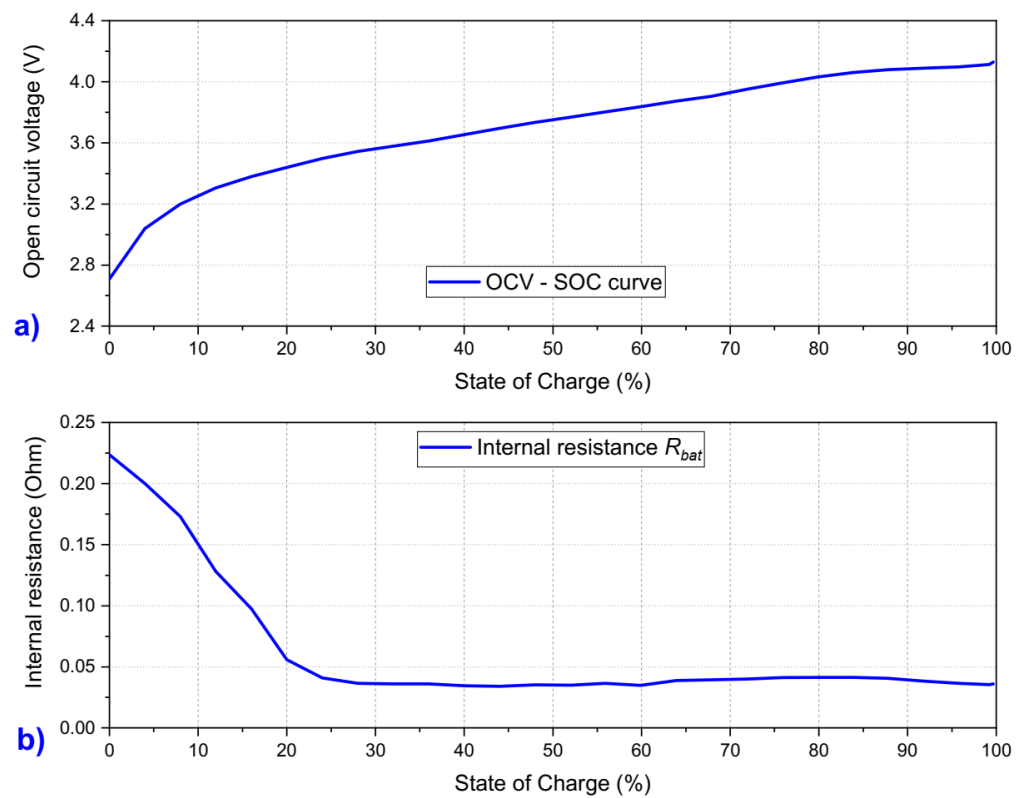


Figure 5. (a) Battery OCV–SOC curve; (b) internal resistance curve.

Table 3. Battery working modes.

SOC Level	Battery Power Level	Definition
$SOC \leq SOC_L$	Very low battery power	Charge priority mode
$SOC_L < SOC \leq SOC_M$	Low battery power	Charge sustaining mode
$SOC_M < SOC \leq SOC_H$	Medium battery power	Charge sustaining or depleting mode
$SOC_H < SOC$	High battery power	Charge depleting mode

3.3. Power Electronics and Other Components Modelling

The performance of the hybrid system is also affected by the efficiency of the power electronic equipment. To reduce the complexity of the system modelling progress, the model of power electronic components of the AC grid such as transformers, DC/AC converter, AC/AC converters, and other devices are represented by an efficiency factor, η_{pe} . As a result, the actual output power of the AC grid is therefore defined as follows:

$$P_{act} = P_{out}\eta_{pe} \tag{9}$$

where P_{act} and P_{out} are, in turn, the output power of the grid after and before considering the efficiency of the power electronic components η_{pe} , respectively.

4. Energy Management Strategy Development

In this section, the EMS control strategies of the hybrid system are developed to control and supervise the power flows amongst the two DGs and the battery pack according to the variation of load command, power level, and operating constraints between the DG and the battery. The objectives of the EMS are to minimize the fuel consumption and thus exhaust gas emissions while maintaining the performance of the system and to maximize the utilisation of the battery within the hybrid system while continuing to prevent it from exceeding the safety pre-set SOC range. In these strategies, the output power of the DG and battery is the control variable, while the power split defining the power distribution between two DGs and the battery pack is the control input of the system.

Rule-based control systems have been widely developed for the automotive sector and other smart grids in the literature [35–37]. They possess several advantages, such as being simple in structure, steady response, and fast switching amongst various operation modes according to different load demands and control scenarios. Theoretically, the algorithm of the rule-based control strategy is easy to implement and suitable for real-time management. However, the transition amongst operation modes in the hybrid system is mostly dependent on the pre-designed switching condition or control criteria such as total power request, constraints of engine start/stop duration, actual battery SOC, and remaining energy in the battery pack. Additionally, the decision of the power split in each mode is mostly dependent on the designer's experiences in understanding the operational behaviour of the vessel and the way to construct the switching rules for the EMS [26].

In this study, the control diagram of the proposed rule-based EMS is depicted in Figure 6. The EMS is established based on two rule sets: the logic for operating mode selection and the logic for power split decision. The first rule set is utilised to select a proper working mode of the vessel according to load demand. Next, the resulting mode and the status of the DGs and battery are fed into the second rule set to define the power split between the DGs and battery. In this figure, the EMS receives the driving command from the load profile, which represents the total operational power request and generates the power request for the two DGs and the battery. The power requests for the DGs are then sent through a procedure to interpolate the torque commands based on their desired operational speed. The power requests for the battery are converted to the current commands based on the actual SOC of the battery. The resulting torque command and current command are finally utilised as the control signals for the ICES and battery, respectively.

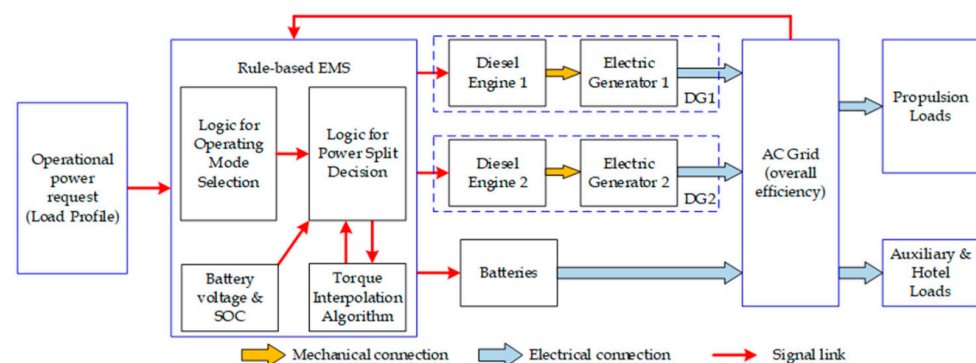


Figure 6. General EMS control diagram of the targeted AC HEMV.

As a result, three rule-based control schemes are finally developed for a non-hybrid vessel and the employed HEMV as follows:

- (1) Control scheme 1 is a conventional DG control strategy (denoted as DGC) developed for the traditional propulsion vessel without a battery pack (non-hybrid vessel). In this strategy, the start/stop duration, operating sequence, and output power of the

DGs are controlled to directly follow the load demands (known as the load following method), disregarding the energy efficiency.

- (2) Control scheme 2 is a standard rule-based control strategy (RBC) developed for the employed HEMV. Conventionally, the RBC is designed based on the power level of the load profile, which is known as the load levelling method, to manage the power distribution amongst the two DGs and battery. Using the RBC concept, the DGs are allowed to operate up to their MOP following the MOL, which provides maximum output power, to track the load demand before requesting power from the battery pack.
- (3) Control scheme 3 is an extended rule-based control strategy (ERBC), which is the expanded version of the RBC, to overcome the limitation of the standard RBC. It is developed based on the load levelling method coupled with the presence of extra function logics to control the operating sequence of the ICE and the start/stop duration of each ICE and manage the power distribution of the two DGs and the battery so that the ICEs can operate at the optimal region while maximising the usage of the battery. As a result, the ERBC allows the ICE to operate at or close to its OOP following the OOL to provide the best fuel economy. By operating the DGs at the OOL, the battery unit can be used more effectively and productively to maintain the overall system performance.

The drawback of the standard RBC strategy is that the ICE, and thus the DG, is usually operating at or close to the MOL. This is not always true, as the higher torque does not improve the fuel saving but conversely leads to the increment of fuel consumption if the ICE keeps running at the high torque region and thus a soaring level of gas emissions. To overcome this issue, the ERBC is considered in such a way to control the DG to operate at or close to the OOL, in combination with the logics to control the ICE operating sequences, start/stop order, and running period to enhance the performance and reduce the overall fuel consumption.

4.1. Representative Operating Load Profile

In the rule-based EMS development process, understanding the characteristics of the operating load profile is very important. Due to the diversity of the operational scenarios of the vessel along with the different power demand level in every voyage, the complexity of the load profile must be considered in the development of a reliable and efficient EMS. To underpin the design and validation of the EMS strategies, a representative load profile based on the characteristic and behaviour of a DP vessel [38] is derived, as shown in Figure 7, where t_i ($i = 1 - n$) and P_j ($j = 1 - m$) are, in turn, the operation time and power request during the voyage, respectively. The load profile represents the total power request, which includes the propulsion power demand and auxiliary and hotel load demand of the vessel. The load profile comprises five operation modes: transit (cruising), DP loading, DP standby, harbour loading, and harbour. Literally, for each voyage, the vessel usually experiences all such working modes, where it consumes low energy at port and depletes high energy when loading, unloading, or cruising. In some specific circumstances, the vessel can turn into any of such DP modes to keep stationary during the journey to transmit merchandise or to perform any particular tasks, for example. Therefore, the efficient EMS control strategy of a hybrid DP system must have the capability to flexibly switch the system amongst those operation modes, control the performance of the propulsion system and the ESS, and manage the power flows between them efficiently.

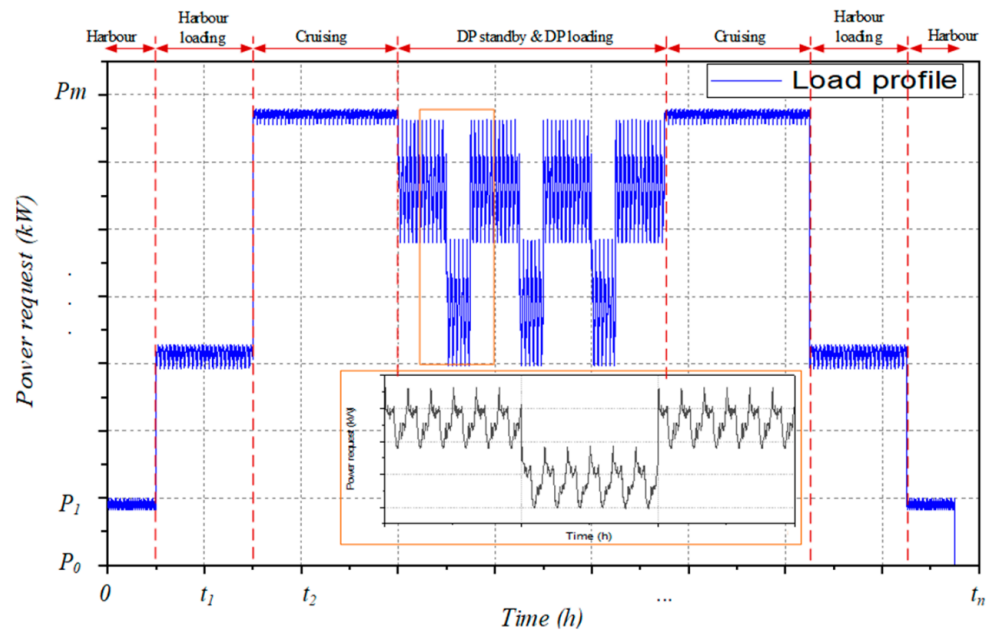


Figure 7. A representative load profile of a DP vessel.

4.2. Power Level Definition

According to the normal operational characteristics of the selected DP vessel and the power capacity of the two DGs and battery, four levels of power request (P_R) are defined, allowing the system to operate within four different power levels as shown in Table 4. The power thresholds are defined as follows:

$$\begin{cases} P_L = 0.5(P_{ICE}^{opt} + P_{ICE}^{max}) \\ P_M = P_{ICE}^{max} + 0.5P_{BAT}^{max} \\ P_H = 2P_{ICE}^{max} \end{cases} \quad (10)$$

where, P_L , P_M , and P_H are in turn the power request, low-power threshold, medium-power threshold, and high-power threshold of the load demand; P_{ICE}^{opt} and P_{ICE}^{max} are in turn the engine optimal and maximum power at a certain speed; P_{BAT}^{max} is the maximum power of the battery.

Table 4. Power level and vessel switching mode definition.

Power Request	Power Level	Vessel Mode Definition
$P_R \leq P_L$	Very low power request	Harbour
$P_L < P_R \leq P_M$	Low power request	Harbour loading + Harbour
$P_M < P_R \leq P_H$	Medium power request	DP standby + DP loading
$P_R > P_H$	High power request	Cruising

where P_R is the instantaneous power request.

It is noteworthy that the values of the power levels are defined as the same for all control strategies. When evaluating the DGC, the battery is not being used in the vessel; the battery maximum power and the initial SOC are set to zero to remove the effect of the battery. In evaluating the RBC and ERBC, to avoid continuous switching between working modes, a small value is added to the thresholds of the battery SOC.

4.3. Operational Constraints

The following constraints have been adopted to maintain the system performance and stability and improve the operational lifetime of the equipment.

Battery useful operational range: the battery charging and discharging current and the operational SOC level are limited for safety reasons. As the output voltage of the battery is varied within its operational range, the input and output power of the battery are also limited. The constraints for the charging/discharging current and SOC variation versus time are as follows:

$$\begin{cases} I_b(t) \leq I_{ch}^{\max} \text{ for charging} \\ I_b(t) \leq I_{dis}^{\max} \text{ for discharging} \\ SOC_{\min} \leq SOC(t) \leq SOC_{\max} \end{cases} \quad (11)$$

where, I_{ch}^{\max} , I_{dis}^{\max} , and $I_b(t)$ are, in turn, the maximum charging current, maximum discharging current, and instantaneous battery current (A); SOC_{\min} , SOC_{\max} , and $SOC(t)$ are, in turn, the minimum limit threshold, maximum limit threshold, and instantaneous SOC of the battery (%). In this study, the negative current stands for the charging current and the positive one represents the discharging one; the SOC_{\min} and SOC_{\max} thresholds are set to 30% and 95%, respectively.

The instantaneous and maximum output power of an ICE unit is also limited and defined as follows:

$$0 \leq P_{ICE}(t) \leq P_{ICE}^{\max} \quad (12)$$

where $P_{ICE}(t)$ and P_{ICE}^{\max} are the instantaneous and maximum output power of the ICE.

Load command conditions: as mentioned, when the load command is larger than or equal to two times the maximum DG output power, the system will be controlled in high power level mode, as shown in Table 4. In this mode, the energy deficit will be compensated by the energy remaining in the battery. Therefore, the maximum load command (P_{load}^{\max}) to which the system can respond is defined as follows:

$$0 \leq P_{load}^{\max} \leq 2P_{ICE}^{\max} + P_{BAT}^{\max} \quad (13)$$

To improve the fuel economy, as well as to minimise the electrical power consumption in starting the ICE, and avoid the high engine start/stop frequency during the journey, once a DG is started, it should be kept running for at least a pre-set duration (ΔT) and can be expressed as follows:

$$t_{ICE}^{ON/OFF} \geq \Delta T \quad (14)$$

4.4. EMS Control Strategies Development and Justification

4.4.1. Conventional Diesel-Generators Control Strategy (DGC)

DGC is designed for the traditional non-hybrid vessel in which the battery unit is not presented. It solely controls the power flow and the operational sequence of two DGs; thus, the total power request distributing to two DGs only follows the load demand disregarding energy efficiency, fuel consumption, and gas emissions. Depending on the power demand, the DGC produces the control signals including the power request and start/stop signal for each DG so that the total output power generated by the two DGs meets the power requirement. Figure 8 shows the block diagram of the DGC strategy, where ICE₁ and ICE₂ stand for diesel engine 1 and 2, respectively; ICE = ON, ICE = OFF are, in turn, to turn on and off the engine, respectively; P₁ and P₂ are the instantaneous power request of the DG₁ and DG₂, respectively.

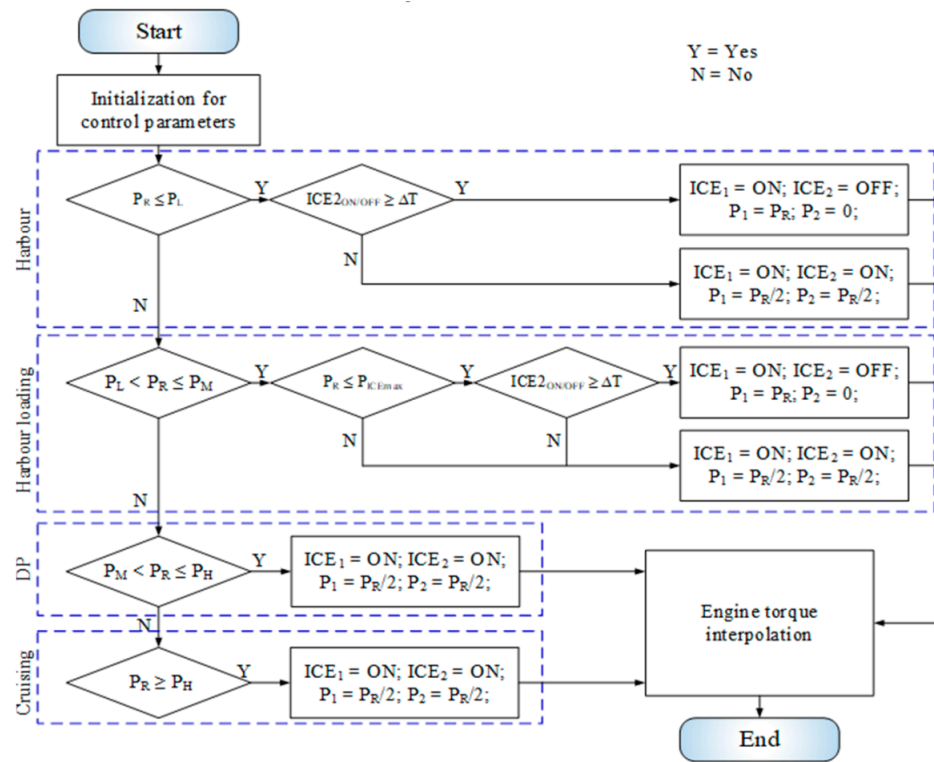


Figure 8. Conventional DGC control block diagram.

4.4.2. Rule-Based Control Strategy (RBC)

RBC is designed for the HEMV based on the power levels of the load profile and the operational mode switching rules, as shown in Equation (10) and Table 4. Once the output power of each DG is controlled up to its maximum power, then the battery depletes additional energy to support the system or accumulates excess energy from the system. In this strategy, the battery pack plays an important role in optimizing the energy of the DGs. The following rule-based logics are employed in order to achieve the control target.

Rule 1: If P_R is less than or equal to P_L .

Then, if the remaining energy in the battery is sufficient to support the system within a pre-set operating duration, two DGs are kept “OFF” and the battery is depleted to support the system; else, when the battery energy is lower than 75% SOC, one DG is started and kept “ON” at the MOP. In this circumstance, the battery accumulates the excess energy from the system for later usage.

Rule 2: If P_R is larger than P_L and less than or equal to P_M .

Then, only one DG is started and kept “ON” so that the output power is up to MOP. The battery is switched to charging or discharging mode according to its required power and SOC status. In this case, the battery SOC is limited so that it can be charged up to 95% (top threshold) or discharged up to 70% to maintain the performance of the battery.

Rule 3: If P_R is larger than P_M and less than or equal to P_H .

Then, depending on the load demand and current battery SOC, one DG or two DGs are turned “ON” and kept running so that the DG’s output power is up to MOP. The battery SOC thresholds are set the same as in Rule 2. When the battery SOC reaches the bottom threshold, it is switched to charge mode, and both DGs are started. In this circumstance, the output powers of both DGs are kept “ON” at the same power output to balance the performance of two DGs.

Rule 4: If P_R is larger than P_H .

Then, two DGs are turned “ON” and held working at MOP; the battery is discharged to the target SOC thresholds, which is stated in Equation (11). Once the battery SOC reaches the bottom threshold (e.g., 30%), the battery is switched “OFF” and thus there are only two DGs operating at MOP. Therefore, the maximum output power of the system in this case is estimated by the total power generated by the two DGs and the maximum discharging power of the battery.

4.4.3. Extended Rule-Based Control Strategy (ERBC)

On RBC, it can be seen that two DGs are priority controlled up to their MOP before depleting the energy from the battery in most of the cases. This leads to the fact that there is significant unnecessary excess energy generated by the DGs that will then be stored in a limited battery capacity. It is therefore increasing the amount of fuel feeding to keep the ICE “ON”, thus increasing fuel consumption and gas emission, while the useful utilisation of the battery is restricted. Consequently, to overcome the weakness of the RBC, ERBC is proposed and applied. ERBC strategy essentially employs the same logics of the RBC, however, by using the load levelling concept with additional function logics to control the ICEs operating at or close to the OOP, following the OOL, to achieve the highest energy efficiency and maximise the utilisation of the battery. In this strategy, the torque command of the ICEs is interpolated based on actual ICE power request and their desired speed so that the total output power is close to the OOP before requesting power from the battery. Furthermore, extra function logics are integrated into ERBC in order to control the ICE operating sequences, which firstly prioritise the single ICE to operate at OOP and then both ICEs at the same working point depending on the power request. This behaviour prevents the ICE from being started/stopped regularly to diminish the influence of the ICE transitional period and the sensitivity of the start/stop function. Additionally, the logics also avoid the operating modes from switching frequently to maintain the stabilisation and reliability of the system. The detailed block diagram of the ERBC strategy is illustrated in Figure 9, where P_{ICEopt} is the optimal power output of the ICE; P_{BAT} is the instantaneous input/output power capacity of the battery according to the charge mode (BAT charged) and discharge mode (BAT discharges) of the battery, respectively.

It is noteworthy that the ERBC maximises the utilisation of the battery and keeps one or both ICEs operating at their OOPs depending on actual power demand. The battery in this strategy can function optimally, and its SOC is varied within its boundaries. It can be used to store the excess energy whenever the supply energy is higher than the demand or feed its energy back to the main grid to support the ICEs when the current energy is smaller than the demand. Furthermore, based on the constraints of the power level switching as in Table 4, and the operational rules and the SOC boundary limits as in Equation (11), the ERBC can fully control the ICEs and manage the battery SOC so that they can operate within the limits. Hence, this EMS strategy can increase the resiliency of the battery SOC whenever the excess energy is positive while maintaining the overall system performance to meet the load requirement.

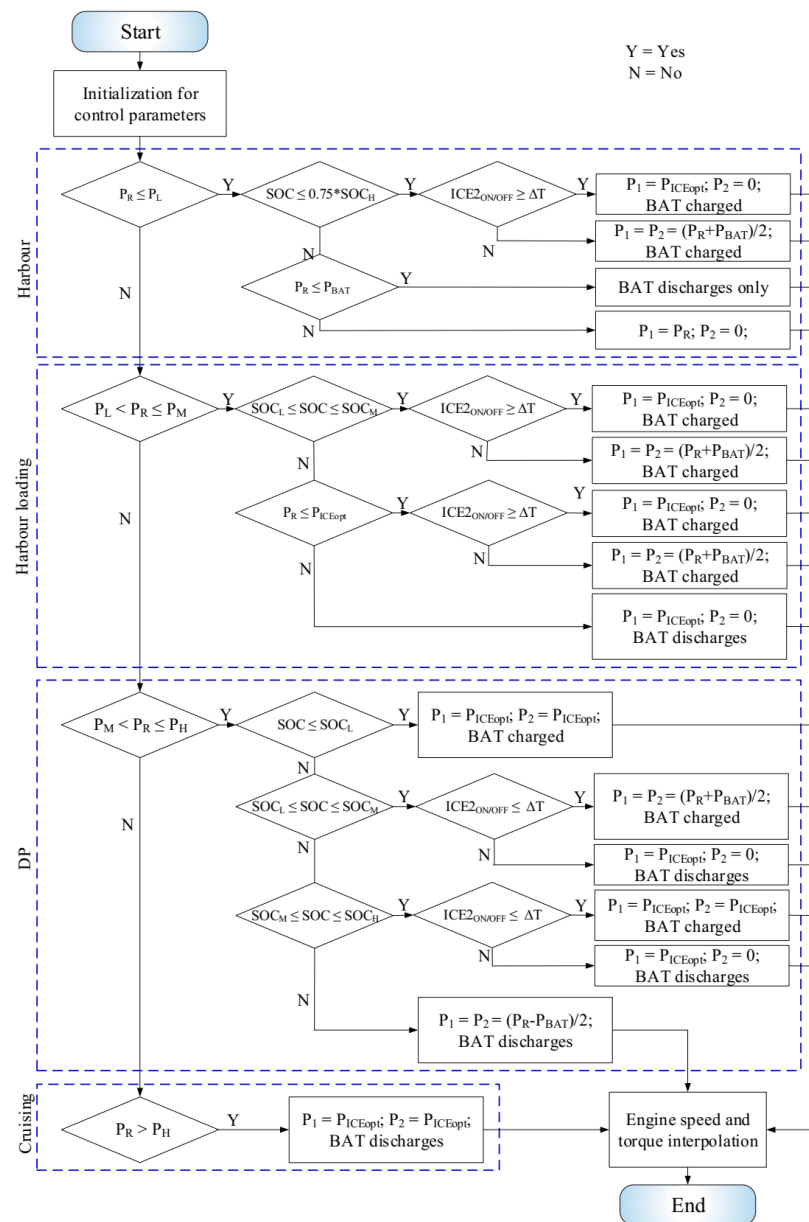


Figure 9. ERBC control block diagram.

5. Real-Time HIL Configuration for Complete HEMV Evaluation

5.1. HIL Platform Definition

To represent the complete DP HEMV system, a HIL simulation platform is built by employing multiple pieces of real-time equipment in combination with the models of key components to simulate the whole system. Figure 10 illustrates the complete system configuration and signal connection. Basically, the platform consists of a SCALEXIO, a MicroAUTOBOX II (MAB), a Battery Simulator (BAT-S), which is manufactured by dSPACE GmbH, a local management unit (LMU) from Texas Instruments, and other peripheral devices that are used for physical signal communication and transmission. The main tasks of each real-time machine can be explained as follows:

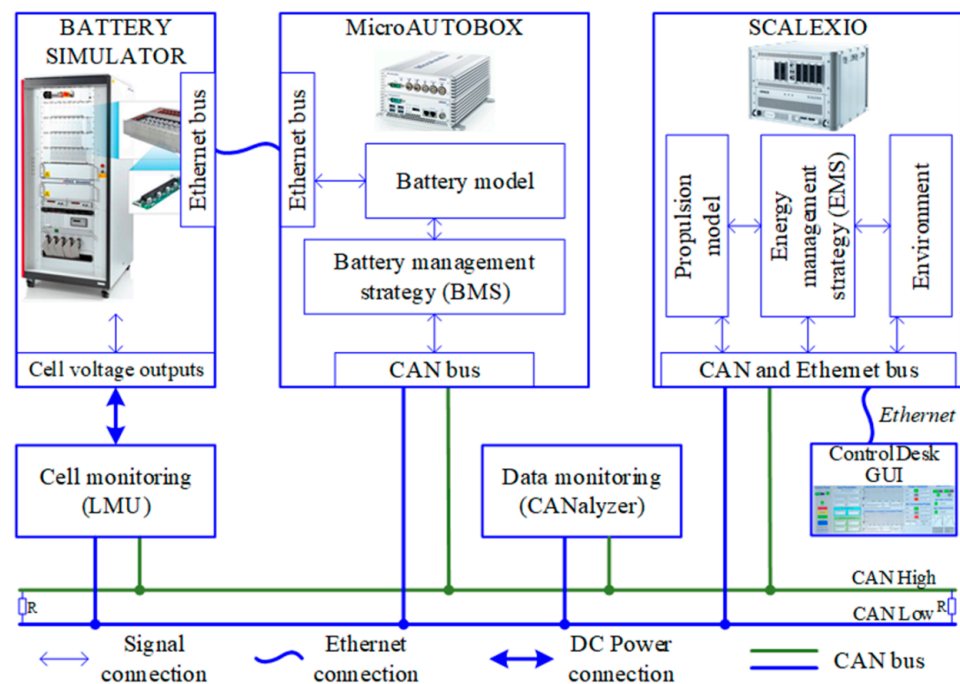


Figure 10. HIL platform communication block diagram.

SCALEXIO is utilised to simulate the complete HEMV system excluding the battery pack based on the developed models as well as to represent the EMS based on the control strategies. In addition, the load profile illustrates that the total power request of the vessel is loaded into this machine to support the system verification. Once the load profile is generated, the EMS then regulates the power split signals for the DGs and the battery pack based on their individual control logic. The control signals for each DG and battery are interpolated accordingly and sent to the targets via a common controller area network (CAN) bus. To demonstrate physical signal transmission amongst EMS, ICE, DG, and battery, all control or feedback signals will be populated into the common system CAN bus; then, they will be delivered or received accordingly by their terminals.

BAT-S is a controllable power electronic device that can simulate a single or multi-cell battery pack based on any kind of mathematical battery model. It can output physical cell voltage with high precision based on the given voltage command from the battery model. This device is ideal to represent a physical battery module or pack for the developing and testing of battery management systems (BMSs) or evaluating the performance of EMSs. In this study, the BAT-S is used to generate physical signals of a battery sub-module 16S1P configuration as described in Section 3.2. The BAT-S is controlled by the MAB via an ethernet bus protocol.

MAB contains the battery model and the BMS algorithm to represent the complete BSS. It is mainly employed to generate the control signals for the BAT-S to simulate the physical battery pack and execute the BMS functions to manage the whole virtual BSS. It is also used to transmit the battery information to the main control unit. Initially, the MAB receives the battery current command, which is the input to the battery model, from the common CAN bus. The battery model then generates the driving command for the BAT-S, which is the cell voltage command, enabling the BAT-S to output physical cell voltages. As mentioned, a 16S1P configuration battery sub-module is generated to simulate the complete scaled-up battery pack. Thereby, once the battery is simulated, all cell information will be physically captured by an LMU where the cell voltages will then be measured, filtered, and broadcasted to the common CAN bus. This information will be once again captured by the MAB for further analysis at the BMS. As the result, the physical output power and parameters of the battery such as cell, module, and pack voltages, driving current, and battery SOC are measured, calculated, and estimated accordingly by the BMS. Finally, the

battery information received from the BMS allows the EMS to determine a suitable decision for the battery, ICE, DG, and overall system. The Matlab/Simulink models developed for the SCALEXIO and MAB are depicted in Figures A1 and A2 in Appendix A, respectively.

In order to monitor the physical cell voltages of the battery pack generated by the BAT-S, LMU is utilised as a measurement device to capture the physical information of the simulated battery. The LMU consists of a battery evaluation board named Ti-BQ76PL455EVM from Texas Instrument and a CAN converter to communicate with the system CAN bus. The role of the battery evaluation board is to capture all physical cell voltages generated by the BAT-S in real-time and transmit to the central BMS over the common CAN bus. Figure 11 depicts the actual HIL simulation platform setup of the real-time HEMV system.

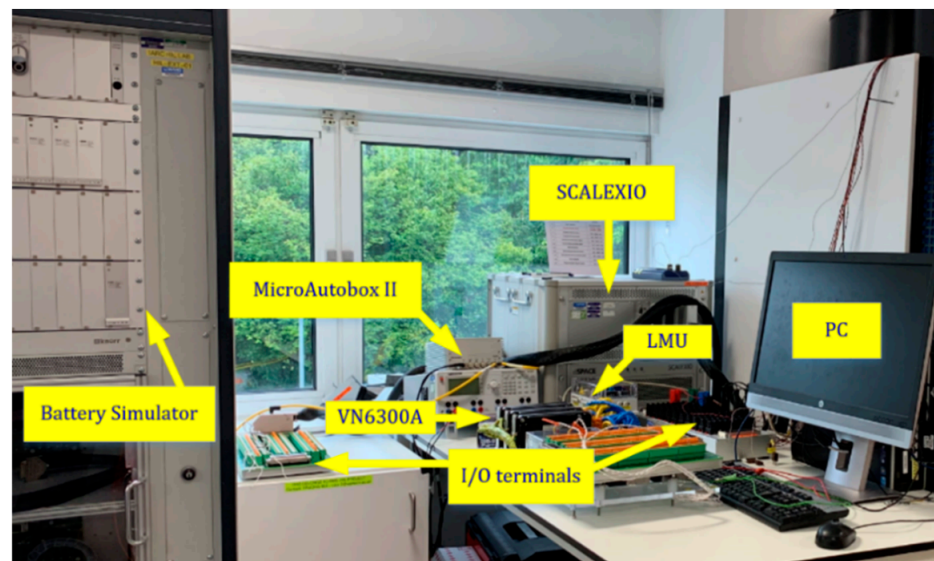


Figure 11. Actual HIL simulation platform setup.

5.2. System Communication Interfaces and Challenges

Unlike offline model-based simulation techniques, a real-time HIL simulation method requires a number of physical communication interfaces for signal exchange between different real-time components. As shown in Figure 10, there are different communication interfaces within the platform for signal transmission such as the CAN bus, Ethernet bus, analogue/digital (A/D) input/output (I/O), and DC power bus where the physical signals can be transmitted or received. The CAN bus is designed to allow various electronic-based devices to exchange their information or signals with each other over a common serial bus. It reduces the wiring harness between devices, thereby reducing the wiring bulkiness and complexity of the complete system. In this configuration, a Vector CANalyzer device (model VN1630A) is installed to monitor and record all CAN signals transmitted within the common CAN bus for post-processing purposes. The details of the CAN signals and messages definition can be seen in Table A1 of Appendix A. As aforementioned, the BAT-S, via Ethernet bus protocol, receives the driving commands from the MAB, in which the battery model and BMS are simulated, to reproduce the physical cell voltages of the battery pack. The physical cell voltages, which are the analogue signals representing the actual terminal voltage of the battery cells, are then captured by the LMU. The LMU receives and broadcasts the cell data to the common CAN bus accordingly.

In fact, during the HIL implementation, it was observed that the communication errors and signal noises occurring due to physical connection are unavoidable. For example, in CAN communication protocol, all signals transmitted amongst components are packed and unpacked according to the magnitude and resolution of the signals. Depending on the priority criteria of the designer, the signal accuracy can be adjusted to fit into a CAN

message and determine how fast the signal can be broadcasted or triggered. These issues significantly affect the accuracy, latency, and update rate of the exchanged signals. In general, it can be summarised as follows:

- (1) Signal resolution and its accuracy: this can be caused by the measurement hardware and the way to transmit and/or receive the signals. While measuring analog signals, depending on the resolution of the analog-to-digital converter (ADC) of the measuring instruments and the signal magnitude or their operating range, the measured signals can be presented within a specific resolution. In addition, performing signal exchanging via CAN bus, all signals need to be “resized” into suitable bit-length so that they can be fitted into predefined messages. This task causes a difference in the accuracy between the original signals and the actual transmitted one. Therefore, depending on the requirement of the accuracy of the signal, the designer can define a suitable resolution for each signal.
- (2) Signal latency and time-shift: this happens in real-time operation activities when a signal is transmitted or received from different devices; the signal can be held for one or several time-steps due to the pre-set sample rate of the model or the priority of the employed hardware. This can lead to the fact that the sent or received signals are being held, delayed, or time-shifted.
- (3) Measurement inaccuracy, noise, and power loss through the power electronic components: these un-avoided drawbacks usually happen when examining analogue signals using electronic measurement equipment.

6. Experimental Results and Discussion

In this section, comparative test-cases of the complete HEMV system are carried out to evaluate the control performance of the proposed ERBC with those of the RBC and DGC on the designed real-time HIL-based HEMV system. Thereby, the results can be used to assess the potential improvement of energy cost, fuel consumption, and thus the emissions of the typical marine system. The representative load profile with five operation modes defined in the previous section is employed as the total power request of the whole voyage. The entire duration of the load profile is pre-scaled to 17.5 h, which enables running experimental tests at current laboratory conditions. As a result, the total power request and the operational duration of each mode of the load profile are illustrated in Figure 12. The whole simulation platform is placed in a temperature controllable thermal chamber where the temperature is held constant at 25 °C to maintain the stability of the electronic systems during the test. To enable and evaluate the control performance comparison in different operating conditions, the system is conducted with two different parameter sets of the ICE minimum operation duration, i.e., 10 and 20 min, and two different initial SOC of the battery, i.e., 85% and 40%, while the rest of the system parameters shown in Tables 1 and 2 are configured the same for all test-cases. As a result, ten test-cases with different control strategies and initial parameter sets are generated, as shown in Table 5. The overall sampling rate is fixed at 10 milliseconds for all test-cases.

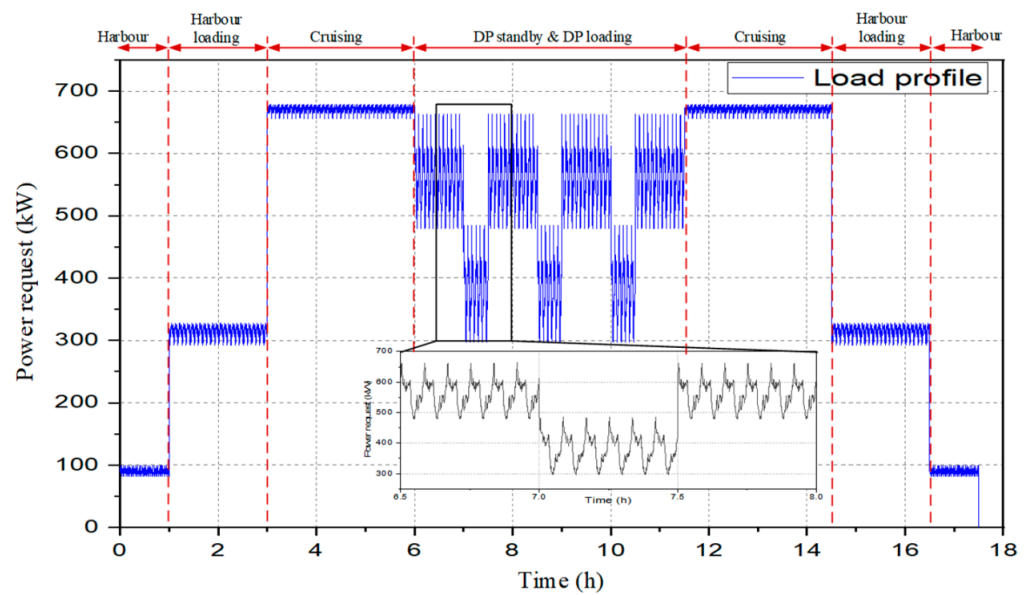


Figure 12. A representative load profile of the HEMV.

Table 5. Test-cases definition.

Test-Cases	Controller (EMS)	Minimum ICE Start/Stop Duration (Minute)	Initial SOC (%)
1	DGC	10	-
2	DGC	20	-
3	RBC	10	85
4	RBC	10	40
5	RBC	20	85
6	RBC	20	40
7	ERBC	10	85
8	ERBC	10	40
9	ERBC	20	85
10	ERBC	20	40

First, test-case 7 is randomly chosen as the representative case within the four test-cases of ERBC to evaluate the applicability of the proposed control strategy in real-time testing conditions. Correspondingly, the necessary output power of the complete HEMV system is estimated in comparison to the total power demand, as shown in Figure 13. The total necessary power is predicted to be higher than the power demand at any certain time of the journey. This behaviour reflects the overall system efficiency including that of the propulsion system (represented by the ICE and DG’s operating efficiency), battery storage (BSS’s efficiency), and overall efficiency of the power electronic and other components. The difference between the total power request and the estimated required power output is shown in the bottom sub-plot of this figure; it shows that a higher power request may obviously lead to a larger difference between the two powers.

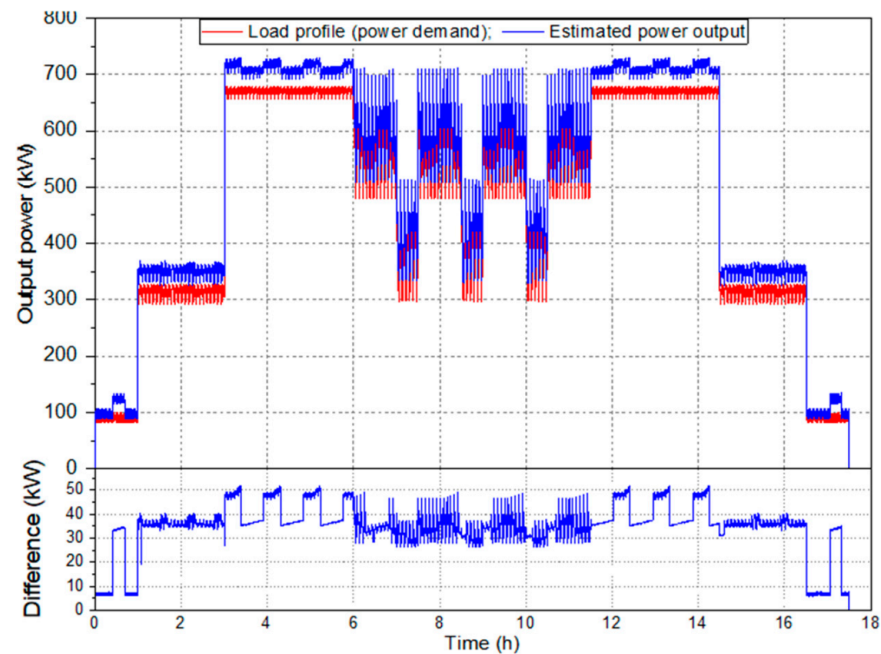


Figure 13. Load profile and estimated necessary power of the HEMV.

Figure 14 depicts the variation of the battery SOC over time, which demonstrates the utilisation performance of the battery during the journey. The battery pack is controlled to be charged or discharged according to the actual power request generated by the ERBC controller. The SOC variation satisfies the safety constraints, as it is altering within the range between 30% and 95% of SOC. In addition, Figure 15 illustrates the battery input power (in charged mode—negative part) and output power (in discharge mode—positive part) variation over time. The results show that the HIL-based battery pack performs very well in real-time and the LMU unit can successfully capture the battery information and send it to the central BMS, and then the EMS, to represent the behaviour of the physical battery system. Consequently, this simulation method provides a capability of validating the control performance of the controllers and allows the testing of the overall HEMV system in a real-time environment.

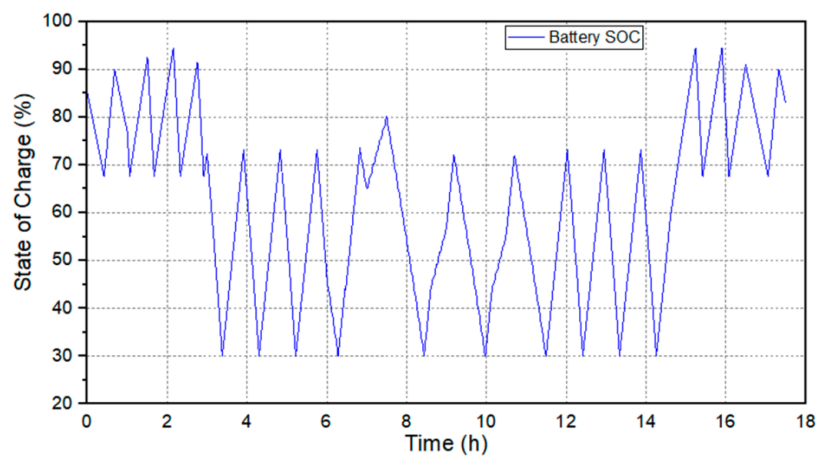


Figure 14. Variation of battery SOC during operation.

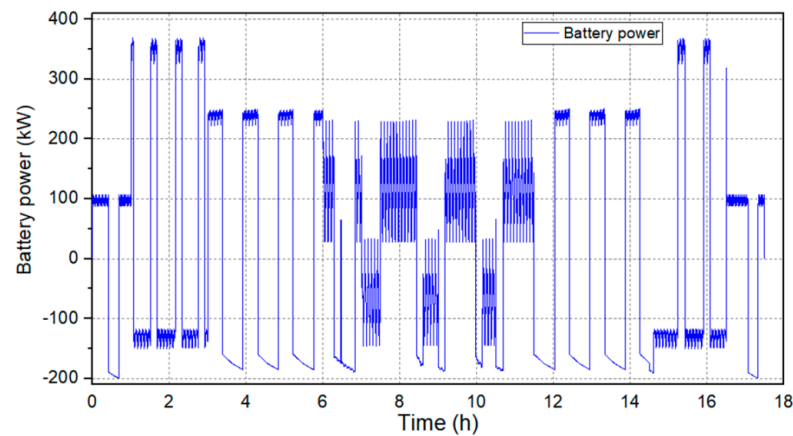


Figure 15. Battery power variation during operation.

Additionally, Figure 16 illustrates the operating performance of the two ICEs and thus the DG's output powers. The top sub-plot shows the start/stop sequences and the operation duration of the ICE. The minimum start/stop duration satisfies the constraint of this test-case; the ICE should operate at least 10 min before stopping. The DG1 has eight start/stop cycles with a stop ratio of 13.59%, while the DG2 has 13 with a 72.57% stop ratio. The bottom sub-plot presents the output power of the DG1 and DG2 according to the ICE start/stop sequences. Both DG1 and DG2 can be turned on and/or off during the voyage to minimize the ICE operation time and thus the fuel consumption and maximize the utilisation of the battery. Once turned on, the DG1 is controlled as close as possible to the OOP while the DG2, if turned on, is controlled so that the output power is the same as that of the DG1 to balance system performance.

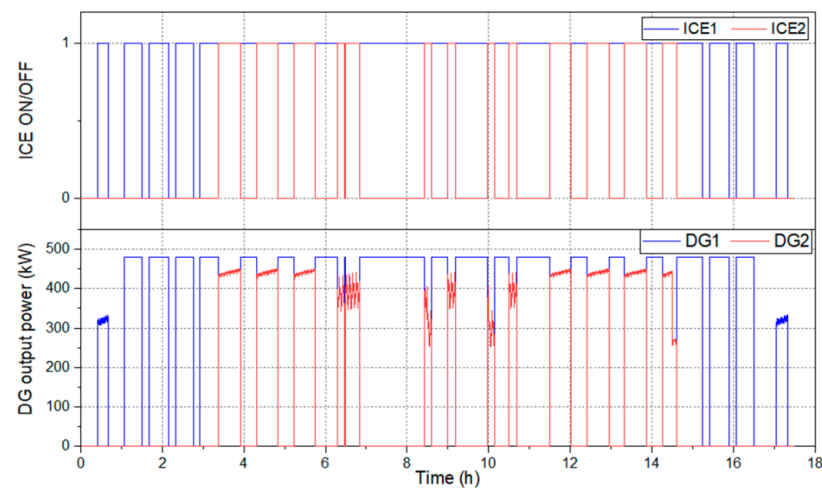


Figure 16. DGs working performance in HIL simulation.

Second, to demonstrate the performance improvement of the proposed ERBC over other control strategies, the key performance indicator (KPI) table is built based on the controller design requirements, as depicted in Table 6. The KPI table enables the comparison of the performance of the HEMV system under three different control approaches in a number of criteria such as the number of ICE start/stop cycles, total operation time per voyage of ICE and DG, fuel consumption, electrical consumption, and energy cost. It is noted that the vessel energy cost is the total cost of fuel consumption, electrical cost for cranking the ICE, and electrical cost, which produces the difference between the initial and final battery SOC. In this table, test-case numbers 1, 3, and 7, which are the representatives of each control strategy, are selected for the comparison. In these test-cases, the minimum start/stop duration of ICE is set to 10 min, while the initial battery SOC is set to 85% for both

RBC and ERBC. The total fuel consumption of the ERBC is saved up to 125 l (equivalent to 4.87%) and 4.818% of the overall energy cost compared to those of the conventional non-hybrid vessel, which uses the DGC. In addition, the results in Table 6 also indicate that the fuel consumption improvement of the ERBC is 11.6l (equivalent to 0.47%), and there is a difference of 0.38% in energy cost saved as compared to the one of the RBC control strategy.

Table 6. KPI comparison of test case number 1, 3, and 7.

KPI	Unit	Conv. Vessel	Hemv	Hemv
		Test Case 1	Test Case 3	Test Case 7
		DGC	RBC	ERBC
Total Run Time	hh:mm:ss	17:30:00	17:30:00	17:30:00
DG 1 Stop/Start Count	-	1	9	8
DG 1 Run Time	s	63,000	54,480	54,432
DG 1 Stop Ratio	%	0	13.52	13.59
DG 2 Stop/Start Count	-	20	9	13
DG 2 Run Time	s	36,089	18,600	17,276
DG 2 Stop Ratio	%	42.68	70.47	72.57
Battery SOC Drop	%	-	-1.04	2.08
Vessel Fuel Used	L	2568.1	2454.7	2443.1
Vessel Fuel Cost	£	3223	3080.6	3066.1
Vessel Elec Used	kWh	-	-2.52	5.0
Vessel Elec Cost	£	10.4	8.6	11.52
Vessel Energy Cost	£	3233.4	3089.2	3077.6
Energy Cost Saved vs DGC	%	-	4.458	4.818
Energy Cost Saved vs RBC	%	-	-	0.38

The ICE fuel consumption is calculated based on the integration of the time-variant BSFC rate over time. In terms of lowering the fuel consumption to reduce the exhaust gas emission, the ICE running at the OOP is preferable. As mentioned, the ERBC controls the ICE to follow the OOL offering the best fuel economy, while the RBC controls the ICE to follow the MOL. This difference can be seen through the actual operational points of the ICE when using the RBC and ERBC, as shown in Figure 17. The red “x” marks and the blue “o” marks represent the actual ICE operating points using the RBC and ERBC, respectively. From the results, within the range of $\pm 5\%$ around the OOP by using the ERBC, the ICE operational point focuses to 64.73%, while there is only 36.79% of the RBC. This concentration shows that the performance of the ERBC is more effective than that of the RBC in driving the system to the suitable operational point. However, it is easy to find out that, with the selected BSFC map in this study, the BSFC rate between the OOP and MOP does not differ significantly, because they are located in the same BSFC level (between the range of 208 and 218 g/kWh in this figure). Therefore, this is the reason why the improvement in fuel consumption by using the ERBC is not significant and thus a small difference in the energy cost is saved in this comparative approach. The fuel consumption improvement could be clearly recognized when the ICE has a large difference in fuel-burning rates between the OOL and MOL.

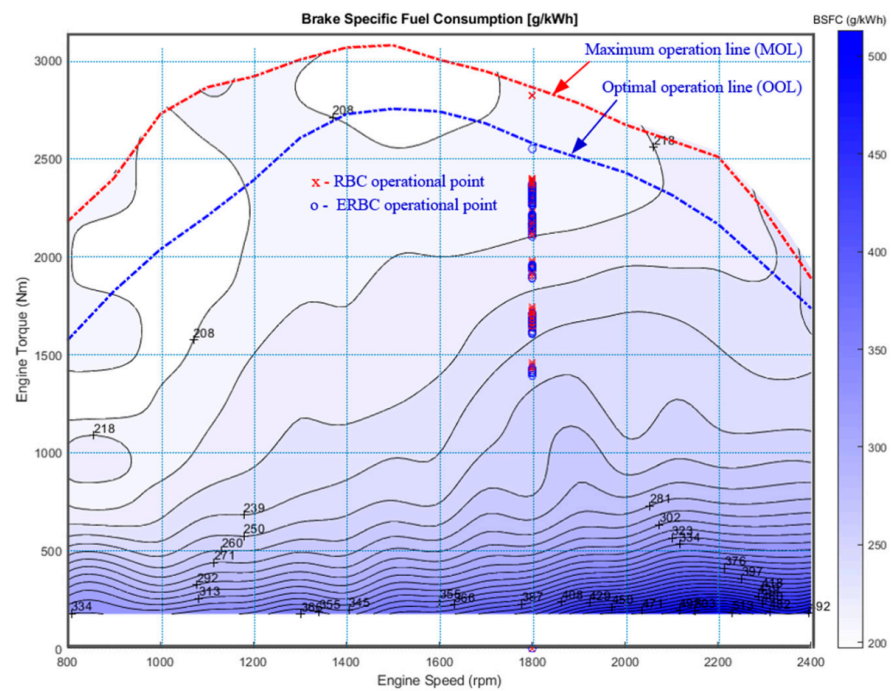


Figure 17. Actual operational point of the ICE under RBC and ERBC.

Finally, a comparison of the ICE fuel consumption and total energy cost of the HEMV using the proposed control strategies is performed and summarised in Table 7. Depending on the initial parameters of the simulation model, the SOC variation, fuel consumption, and thus total energy cost are varied through each test case. In the traditional vessel, the DGC controls the ICEs to follow the power request so these ICEs could not operate within their optimal region. The output power of the ICEs is dependent on the power command and thus the instantaneous fuel consumption rate of the system in this case is varied according to the power level. In the HEMV with the use of a battery, the electrical energy stored in the battery is converted to support the system when needed, while the excess energy of the system is accumulated and stored in the battery. This allows the ICEs to operate up to their maximum or optimum power regions under the control of the RBC and ERBC strategies, respectively. Therefore, the fuel consumption under these control strategies is improved compared to that of the conventional vessels.

Table 7. Comparison of energy consumption under MIL and HIL simulation methods.

Test Cases			Energy Consumption					
No.	CTRL	ICE on Duration	Initial SOC	Final SOC	SOC Drop	ICE Fuel Consumption	Fuel Cost	Energy Cost
-	-	min	%	%	%	L	£	£
1	DGC	10	-	-	-	2568.1	3223.0	3233.4
2	DGC	20	-	-	-	2576.1	3233.0	3239.9
3	RBC	10	85	86.04	-1.04	2454.7	3080.6	3089.2
4	RBC	10	40	82.82	-42.82	2488.6	3123.2	3118.9
5	RBC	20	85	73.39	11.61	2459.4	3086.6	3095.0
6	RBC	20	40	89.75	-49.75	2483.5	3116.8	3110.9
7	MRBC	10	85	82.92	2.08	2443.1	3066.1	3077.6
8	MRBC	10	40	84.12	-44.12	2476.8	3108.4	3105.7
9	MRBC	20	85	89.74	-4.74	2458.1	3084.9	3089.9
10	MRBC	20	40	89.58	-49.58	2480.2	3112.7	3107.3

From the simulation results and discussion, it can be stated that the developed system model is reliable and robust under different testing methods. The system outputs performing within the two methods met each other very well. As discussed, the difference in the performance of key components can be recognised as just the influence of the communication issues when using the HIL method. The real-time simulation results help to predict the performance and response of the actual system in the real world. Additionally, the EMS-based ERBC strategy performs very well and satisfies the control design requirement and constraints. By using this control approach, the ICEs work closely to the OOP to achieve the best efficiency and thus the lowest fuel consumption.

7. Conclusions and Future Works

7.1. Conclusions

In this paper, an ERBC EMS is proposed and validated on a real-time HIL-based DP HEMV system. Map-based performance system models are developed and unified to represent a complete HEMV for the EMS control strategies' development and verification. The KPI comparative results between the developed EMSs and the traditional ones illustrate the improvement in terms of fuel saving and thus gas emission reduction and operational cost minimisation. The result of the validation method underpins the transferability and applicability of the HIL testing technology from the automotive sector into the maritime industry, which will be the premise for complete testing procedures before deploying to a real vessel system.

7.2. Future Works

Beyond the scope of the study, an extended validation of the system performance and evaluation of the ERBC over those of the RBC using actual DGs and a battery pack can be conducted to overcome the limitations of the current HIL simulation platform. The following directions can be potentially considered for the implementation of an HEMV system:

- (1) For the system modelling, a model of the propeller should be considered to capture the behaviours of the propellers of the vessel.
- (2) A full dynamic system model of a DP HEMV should be developed to represent the performance of the system. In this case, different load profiles and working conditions could be applied to investigate the control capability of the designed EMS over different working conditions.
- (3) To consider the influences of the DG performance, especially the ICE operational transient, actual ICE and generators can be employed. Then, actual BSFC efficiency maps of the engine and DG can be incorporated to address the cost issues between the EMS strategies.
- (4) To perform an extended evaluation of the control performance with complex behaviours of the battery such as the transient during charging and discharging and battery degradation, advanced battery models such as high order ECM or electrochemical models can be employed and incorporated into the system model, particularly with the integration of the battery degradation mechanism that can capture the non-linear ageing behaviour of the battery to evaluate the influence of battery ageing on the control performances.
- (5) To evaluate the performance of the battery under the effect of temperature, a temperature model can be developed and integrated into the ECM, or an actual scaled-down battery module operating within controlled climate chamber can be employed.

Author Contributions: Data curation, T.M.N.B. and T.Q.D.; formal analysis, T.M.N.B.; funding acquisition, J.M. and C.W.; investigation, T.M.N.B.; methodology, T.M.N.B.; project administration, J.M. and C.W.; resources, C.W.; software, T.M.N.B. and T.Q.D.; supervision, J.M.; validation, T.M.N.B.; visualization, T.Q.D.; writing—original draft, T.M.N.B.; writing—review and editing, T.Q.D. and J.M. All authors have read and agreed to the published version of the manuscript.

Funding: This research was funded by Innovate UK through the Agile Power Management System (APMS), project number: 102437, in collaboration with the WMG Centre of High Value Manufacturing (HVM), Babcock and Potenza.

Conflicts of Interest: The authors declare no conflict of interest.

Appendix A

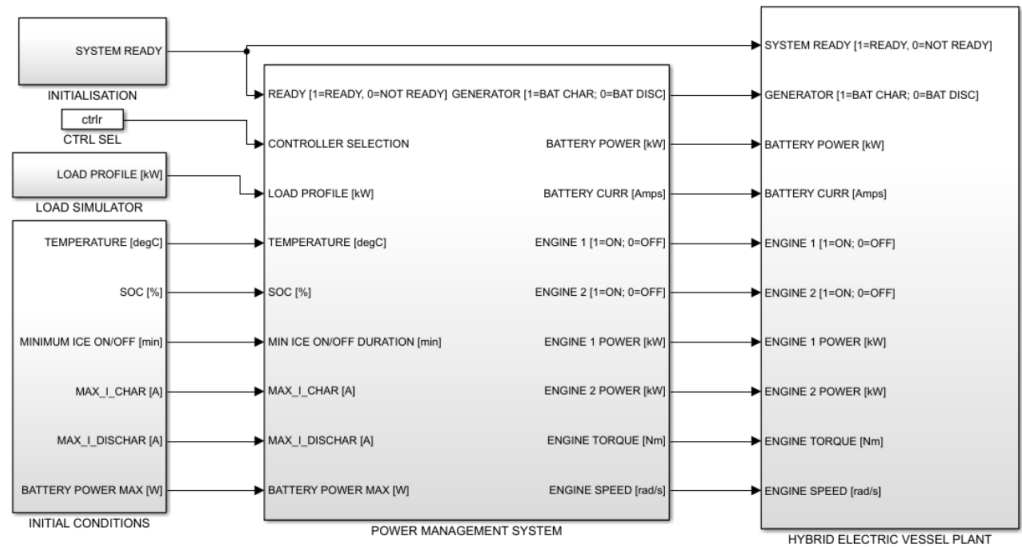


Figure A1. Matlab/Simulink model for SCALEXIO.

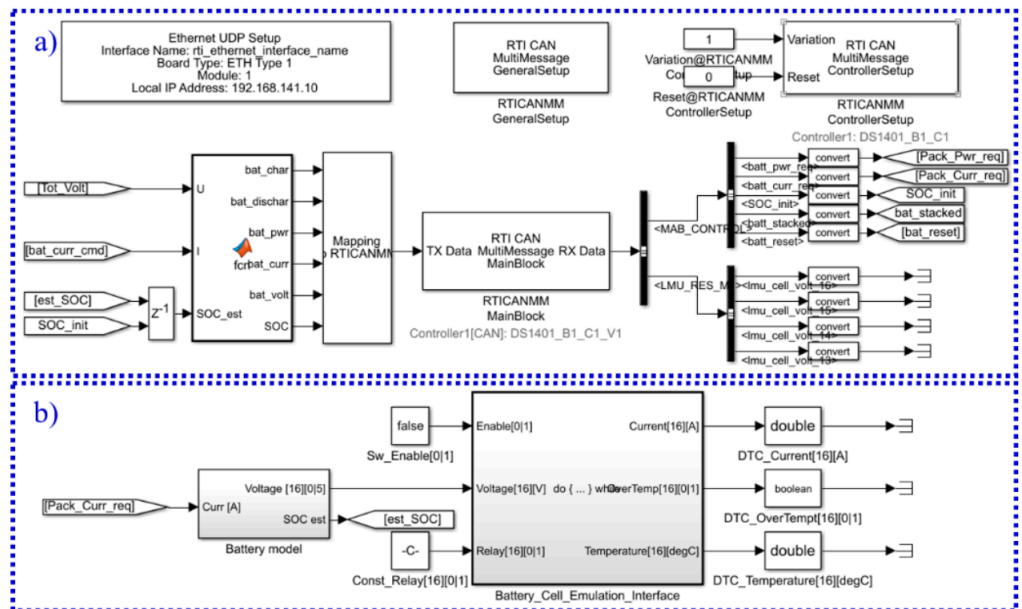


Figure A2. Matlab/Simulink model for MAB ((a) CAN configuration, (b) battery emulation).

Table A1. Definition of CAN messages.

No.	Messages	Signals	Size (bit)	Resolution	Min	Max	Unit
1	LMU_RES_M ⁽¹⁾	Cell_volt_x ⁽²⁾	16	7.63×10^{-5}	0	5	Volt
2	BAT_DATA	Bat_char	1	1	0	1	-
3		Bat_dischar	1	1	0	1	-
4		Bat_pwr ⁽³⁾	18	0.01	-1000	1000	kW
5		Bat_curr ⁽³⁾	18	0.01	-1000	1000	A
6		Bat_volt	13	0.1	0	500	Volt
7		SOC	10	0.1	0	100	%
8		Bat_pwr_req ⁽³⁾	18	0.01	-1000	1000	kW
9		Bat_curr_req ⁽³⁾	18	0.01	-1000	1000	A
10	MAB_CONTROL	SOC_init	10	0.1	0	100	%
11		Bat_stacked	1	1	0	1	-
12		Bat_reset	1	1	0	1	-

^{(1),(2)}: The authors would like to maintain the same accuracy of the cell voltages measured by the employed evaluation board LMU (16 bits resolution); therefore, 4 messages are created (e.g., LMU_RES_M, M = 1–4) where each message contains 4 signals accordingly (e.g., Cell_volt_x, x = 1–16). ⁽³⁾: negative value stands for charging and vice versa.

References

- Serrano, R.J. Imagining the Future of the Internal Combustion Engine for Ground Transport in the Current Context. *Appl. Sci.* **2017**, *7*, 1001. [\[CrossRef\]](#)
- Juric, V.; Zupanovic, D. Ecological impacts of diesel engine emissions. *Hum. Transp. Interact. Rev.* **2012**, *24*, 151–160. [\[CrossRef\]](#)
- Panapakidis, I.; Sourtzi, V.-M.; Dagoumas, A. Forecasting the Fuel Consumption of Passenger Ships with a Combination of Shallow and Deep Learning. *Electronics* **2020**, *9*, 776. [\[CrossRef\]](#)
- Hein, K.; Yan, X.; Wilson, G. Multi-Objective Optimal Scheduling of a Hybrid Ferry with Shore-to-Ship Power Supply Considering Energy Storage Degradation. *Electronics* **2020**, *9*, 849. [\[CrossRef\]](#)
- International-Maritime-Organisation. *Prevention of Air Pollution from Ships*; International Maritime Organization: London, UK, 2009.
- Prpić-Oršić, J.; Faltinsen, O.M. Estimation of ship speed loss and associated CO2 emissions in a seaway. *Ocean Eng.* **2012**, *44*, 1–10. [\[CrossRef\]](#)
- Geertsma, R.D.; Negenborn, R.R.; Visser, K.; Hopman, J.J. Design and control of hybrid power and propulsion systems for smart ships: A review of developments. *Appl. Energy* **2017**, *194*, 30–54. [\[CrossRef\]](#)
- Donato, T.; Spedicato, L.; Pio Placentino, D. Design and performance evaluation of a hybrid electric power system for multi-copters. *Energy Procedia* **2017**, *126*, 1035–1042. [\[CrossRef\]](#)
- Li, Z.; Huang, Y.; Wang, H. A new system configuration design and power management strategies for a multi-source hybrid truck. *Proc. Inst. Mec. Eng. Part I J.Syst. Control Eng.* **2018**, *232*, 1053–1062. [\[CrossRef\]](#)
- Do, T.C.; Tran, D.T.; Dinh, T.Q.; Ahn, K.K. Tracking Control for an Electro-Hydraulic Rotary Actuator Using Fractional Order Fuzzy PID Controller. *Electronics* **2020**, *9*, 926. [\[CrossRef\]](#)
- Moreno, V.M.; Pigazo, A. Future trends in electric propulsion systems for commercial vessels. *J. Marit. Res.* **2007**, *4*, 81–100.
- Skjong, E.; Volden, R.; Rødskar, E.; Molinas, M.; Johansen, T.A.; Cunningham, J. Past, Present, and Future Challenges of the Marine Vessel's Electrical Power System. *IEEE Trans. Transp. Electrification* **2016**, *2*, 522–537. [\[CrossRef\]](#)
- Zhu, W.; Guo, J.; Zhao, G. Multi-Objective Sizing Optimization of Hybrid Renewable Energy Microgrid in a Stand-Alone Marine Context. *Electronics* **2021**, *10*, 174. [\[CrossRef\]](#)
- Jaurola, M.; Hedin, A.; Tikkanen, S.; Huhtala, K. Optimising design and power management in energy-efficient marine vessel power systems: A literature review. *J. Mar. Eng. Technol.* **2019**, *18*, 92–101. [\[CrossRef\]](#)
- Qi, L.; Li, B.; Chen, L.; Wang, W.; Dong, L.; Jia, X.; Huang, J.; Ge, C.; Xue, G.; Wang, D. Ship Target Detection Algorithm Based on Improved Faster R-CNN. *Electronics* **2019**, *8*, 959. [\[CrossRef\]](#)
- Bai, H. Position Estimation of a PMSM in an Electric Propulsion Ship System Based on High-Frequency Injection. *Electronics* **2020**, *9*, 276. [\[CrossRef\]](#)
- Kanellopoulos, D.; Norman, R.A.; Dev, A.K. Investigation into the application of a hybrid propulsion system in an offshore support vessel. In Proceedings of the Singapore Maritime Technology Conference, Singapore, 26–28 April 2017; pp. 1–13.
- Diju, G.; Kangkai, P.; Jianxin, C.; Aidi, S.; Yanyan, S. Control strategy of hybrid electric ship based on improved fuzzy logic threshold. In Proceedings of the 2017 29th Chinese Control And Decision Conference (CCDC), Chongqing, China, 28–30 May 2017; pp. 6995–7000.
- Shagar, V.; Jayasinghe, G.S.; Enshaei, H. Effect of Load Changes on Hybrid Shipboard Power Systems and Energy Storage as a Potential Solution: A Review. *Inventions* **2017**, *2*, 21. [\[CrossRef\]](#)

20. Barreras, J.V.; Fleischer, C.; Christensen, A.E.; Swierczynski, M.; Schaltz, E.; Andreasen, S.J.; Sauer, D.U. An Advanced HIL Simulation Battery Model for Battery Management System Testing. *IEEE Trans. Ind. Appl.* **2016**, *52*, 5086–5099. [[CrossRef](#)]
21. Martínez-García, M.S.; de Castro, A.; Sanchez, A.; Garrido, J. Analysis of Resolution in Feedback Signals for Hardware-in-the-Loop Models of Power Converters. *Electronics* **2019**, *8*, 1527. [[CrossRef](#)]
22. Sanchez, A.; de Castro, A.; Martínez-García, M.S.; Garrido, J. LOCOFloat: A Low-Cost Floating-Point Format for FPGAs.: Application to HIL Simulators. *Electronics* **2020**, *9*, 81. [[CrossRef](#)]
23. Chas, C.S.; Ferreiro, R. Introduction to ship dynamic positioning system. *J. Mar. Res.* **2008**, *5*, 79–95.
24. Rigatos, G.; Siano, P. Robust control of valves in ship diesel engines with the use of the Derivative-free nonlinear Kalman filter. *Proc. Inst. Mec. Eng. Part I J.Syst. Control Eng.* **2014**, *228*, 631–644. [[CrossRef](#)]
25. Bui, T.M.N.; Dinh, T.Q.; Marco, J.; Watts, C. An Energy Management Strategy for DC Hybrid Electric Propulsion System of Marine Vessels. In Proceedings of the 2018 5th International Conference on Control, Decision and Information Technologies (CoDIT), Thessaloniki, Greece, 10–13 April 2018; pp. 80–85.
26. Dinh, T.Q.; Bui, T.M.N.; Marco, J.; Watts, C.; Yoon, J.I. Optimal Energy Management for Hybrid Electric Dynamic Positioning Vessels. *IFAC-PapersOnLine* **2018**, *51*, 98–103. [[CrossRef](#)]
27. JCB_Ltd. DieselMax EcoMax Engine Tier 4 Type 448. 2021. Available online: <https://www.jcb.com/en-gb/products/engines/base-engine/tier-4f-base> (accessed on 1 April 2021).
28. Caterpillar_Ltd. *Caterpillar Marine Engine Tier 4*; Caterpillar Ltd.: Leicester, UK, 2021; Available online: https://www.cat.com/en_US/by-industry/marine/tier-four.html (accessed on 1 April 2021).
29. Zheng, F.; Xing, Y.; Jiang, J.; Sun, B.; Kim, J.; Pecht, M. Influence of different open circuit voltage tests on state of charge online estimation for lithium-ion batteries. *Appl. Energy* **2016**, *183*, 513–525. [[CrossRef](#)]
30. Bui, T.M.; Faraji-Niri, M.; Worwood, D.; Dinh, T.Q.; Marco, J. An Advanced Hardware-in-the-loop Battery Simulation Platform for the Experimental Testing of Battery Management System. In Proceedings of the 23rd International Conference on Mechatronics Technology Salerno, Salerno, Italy, 23–26 October 2019.
31. Niri, M.F.; Bui, T.M.N.; Dinh, T.Q.; Hosseinzadeh, E.; Yu, T.F.; Marco, J. Remaining energy estimation for lithium-ion batteries via Gaussian mixture and Markov models for future load prediction. *J. Energy Storage* **2020**, *28*, 101271. [[CrossRef](#)]
32. Reniers, J.M.; Mulder, G.; Howey, D.A. Unlocking extra value from grid batteries using advanced models. *J. Power Sources* **2021**, *487*, 229355. [[CrossRef](#)]
33. Li, Y.; Vilathgamuwa, M.; Choi, S.S.; Xiong, B.; Tang, J.; Su, Y.; Wang, Y. Design of minimum cost degradation-conscious lithium-ion battery energy storage system to achieve renewable power dispatchability. *Appl. Energy* **2020**, *260*, 114282. [[CrossRef](#)]
34. Bruen, T.; Marco, J. Modelling and experimental evaluation of parallel connected lithium ion cells for an electric vehicle battery system. *J. Power Sources* **2016**, *310*, 91–101. [[CrossRef](#)]
35. Puerto-Flores, D.D.; Scherpen, J.M.A.; Liserre, M.; Vries, M.M.J.d.; Kransse, M.J.; Monopoli, V.G. Passivity-Based Control by Series/Parallel Damping of Single-Phase PWM Voltage Source Converter. *IEEE Trans. Control Syst. Technol.* **2014**, *22*, 1310–1322. [[CrossRef](#)]
36. Sanjari, M.J.; Karami, H.; Gooi, H.B. Analytical Rule-Based Approach to Online Optimal Control of Smart Residential Energy System. *IEEE Trans. Ind. Inform.* **2017**, *13*, 1586–1597. [[CrossRef](#)]
37. Sharma, S.; Lüßmann, J.; So, J. Controller Independent Software-in-the-Loop Approach to Evaluate Rule-Based Traffic Signal Retiming Strategy by Utilizing Floating Car Data. *IEEE Trans. Intell. Transp. Syst.* **2019**, *20*, 3585–3594. [[CrossRef](#)]
38. Bø, T.I.; Johansen, T.A.; Sørensen, A.J.; Mathiesen, E. Dynamic consequence analysis of marine electric power plant in dynamic positioning. *Appl. Ocean Res.* **2016**, *57*, 30–39. [[CrossRef](#)]